# Fast-ion D-alpha measurements at ASDEX Upgrade

**B Geiger[1], M Garcia-Munoz[1], W W Heidbrink[2], R M McDermott[1], G Tardini[1], R Dux[1], R Fischer[1], V Igochine[1] and the ASDEX Upgrade Team**

[1] Max-Planck Institut für Plasma Physik, Garching, Munich, Germany
[2] Department of Physics and Astronomy, University of California, Irvine, CA 92697, USA

E-mail: benedikt.geiger@ipp.mpg.de

## Abstract

A fast-ion D-alpha (FIDA) diagnostic has been developed for the fully tungsten coated ASDEX Upgrade (AUG) tokamak using 25 toroidally viewing lines of sight and featuring a temporal resolution of 10 ms. The diagnostic's toroidal geometry determines a well-defined region in velocity space which significantly overlaps with the typical fast-ion distribution in AUG plasmas. Background subtraction without beam modulation is possible because relevant parts of the FIDA spectra are free from impurity line contamination. Thus, the temporal evolution of the confined fast-ion distribution function can be monitored continuously. FIDA profiles during on- and off-axis neutral beam injection (NBI) heating are presented which show changes in the radial fast-ion distribution with the different NBI geometries. Good agreement has been obtained between measured and simulated FIDA radial profiles in MHD-quiescent plasmas using fast-ion distribution functions provided by TRANSP. In addition, a large fast-ion redistribution with a drop of about 50% in the central fast-ion population has been observed in the presence of a $q = 2$ sawtooth-like crash, demonstrating the capabilities of the diagnostic.

(Some figures in this article are in colour only in the electronic version)

## 1. Introduction

In present fusion devices, fast ions (ions with energies significantly above the thermal energy) are produced by external heating systems such as neutral beam injection (NBI) and ion cyclotron resonance heating (ICRH). Their confinement is essential because fast ions contribute to plasma heating and current drive and can, if poorly confined, even lead to damage of the first wall [1]. Several techniques exist to study the fast-ion confinement, such as fast-ion loss detectors (FILD) [2], neutral particle analyzers (NPA) [3], gamma ray tomography [4], collective

Thomson scattering (CTS) [5], neutron spectroscopy [6] and fast-ion D-alpha (FIDA) [7] measurements. The FIDA technique, which is similar to spectroscopic measurements of fast alpha particles [8], was first implemented at DIII-D [9] and has become a widely used method due to its relatively good spatial and temporal resolution. It is now used as well in TEXTOR [10], LHD [11] and NSTX [12] and has yielded results on the fast-ion distribution due to micro-turbulence [13], Alfven waves [14] and different injection geometries [15].

The FIDA technique is charge-exchange recombination spectroscopy (CXRS) [16]) applied to fast D-ions. Through charge-exchange reactions with neutrals, the fast ions can capture an electron into an excited quantum $n$-level, become neutral themselves, and subsequently emit line radiation. The radiation is typically emitted before the neutralized fast ions (fast neutrals) move more than a few centimeters as the de-excitation back to the equilibrium happens very quickly. Several spectral lines from the fast neutrals exist in fusion plasmas; however, FIDA measurements tend to use the Balmer alpha emission line ($\lambda_0 = 656.1$ nm, $n = 3$ to $n = 2$). Balmer Alpha radiation permits the use of standard lenses and spectrometers as it is in the visible range. The FIDA emission is localized mainly along the path of the NBI as there is no significant overlap of fast ions and neutrals elsewhere. Hence, multiple lines of sight (LOS) that intersect neutral beams at different radii can be used to obtain profile information.

Information on the velocity distribution of fast ions is contained in the spectral shape of FIDA radiation. The shape is dominated by the Doppler effect which depends on the velocity vector of the fast neutrals, $\vec{v}$, or, in other words, on the fast neutrals energy parallel to the viewing direction, $E_\parallel$:

$$\Delta\lambda_{\text{Doppler}} = \lambda_0 \cdot \frac{\cos(\alpha) \cdot |\vec{v}|}{c} \propto \sqrt{E_\parallel}. \tag{1}$$

Here, $c$ is the speed of light, $\lambda_0$ is the unshifted wavelength and $\alpha$ is the angle between $\vec{v}$ and a given LOS. The Doppler effect shifts the D-alpha emission considerably in wavelength. The spectral shape of the FIDA emission has consequently broad spectral wings. It deviates significantly from a Gaussian curve because fast ions do not follow a Maxwell distribution. It should be noted that the nature of the Doppler effect makes an energy and pitch ($v_\parallel/v_{\text{tot}}$, i.e. the projection of $\vec{v}$ on the magnetic field lines) resolved measurement virtually impossible. That is to say, one cannot relate a specific shift in wavelength to a unique energy as fast ions with a higher energy and larger angles $\alpha$ can result in similar shifts.

Information on fast-ion density profiles is contained in the measured spectral radiances. The FIDA radiance is proportional to the density of fast neutrals in the $n = 3$ level present along a LOS. This density depends not only on the fast-ion density, but also on the probability for charge exchange and on the mechanisms that populate the $n = 3$ level. The probability for a fast ion to undergo charge exchange in which the electron ends up in the $n$-level, $i$, is

$$\text{prob}_{\to i} = \sum_j \sum_k n_{\text{NBI}(j,k)} \cdot \sigma_{cx(j\to i)}(v_{\text{rel}(k)}) \cdot v_{\text{rel}(k)} \tag{2}$$

where $n_{\text{NBI}(j,k)}$ is the density of injected and halo neutrals present along the NBI with different $n$-levels, $j$, and energies, $k$, $v_{\text{rel}(k)}$ is the relative velocity between fast ions and neutrals and $\sigma_{cx(j\to i)}$ is the energy-dependent charge-exchange cross section. All of the various neutral beam energy components and $n$-levels as well as the halo population have to be accounted for separately because the charge-exchange cross-sections depend on $n$-levels and energies. The halo neutrals originate from charge-exchange reactions between the injected beam neutrals and the thermal D-ions (the bulk plasma ions). Due to these reactions as well as subsequent charge-exchange reactions of the halo neutrals with thermal D-ions, a cloud of neutrals surrounding the NBI is built whose density is typically comparable to or even larger than the beam neutral

density. The NBI halo density is important for FIDA measurements because the high collision energy between the fast ions and the halo neutrals provides a significant probability for charge-exchange reactions.

A considerable fraction of fast neutrals are in the $n = 3$ level directly after charge exchange. Additionally, the $n = 3$ level can be populated by the radiative decay from higher $n$-levels that have been populated by charge exchange or other mechanisms. Furthermore, fast neutrals in lower $n$-levels can be excited into the $n = 3$ level by collisions along their path through the plasma. This effect yields non-localized FIDA radiation but, fortunately, does not strongly limit the spatial resolution of the technique. The FIDA radiation emitted in the equilibrium (through collisions) is comparably small. The radiation which is emitted directly after charge exchange is more intense as the charge-exchange reaction strongly overpopulates the excited $n$-levels.

The interpretation of FIDA spectra is difficult. In particular, the moderate resolution in velocity space (one cannot resolve information on the energy and pitch of fast ions independently) and the energy-dependent charge exchange cross sections make a direct de-convolution of FIDA measurements to fast-ion distribution functions virtually impossible. However, two different methods can be applied when analyzing FIDA measurements to circumvent this difficulty: first, a forward model can be used to quantitatively interpret FIDA measurements. By simulating the neutralization and photon emission of fast ions that correspond to a given distribution function it is possible to calculate synthetic FIDA spectra. These can then be compared with the measurement. Second, after accounting for changes in the density profiles of injected and halo neutrals, changes in the FIDA data can be interpreted as variations in the fast-ion distribution function. Hence, relative changes of the fast-ion distribution function can be studied, e.g. in the presence of MHD activity.

This paper is structured as follows: section 2 is dedicated to the newly commissioned toroidal FIDA diagnostic. The diagnostic's setup is presented and the observed FIDA spectra and radial intensity profiles are discussed. Furthermore, the diagnostic's velocity space weighting function is discussed. The subsequent sections are devoted to experimental results. Section 3 discusses measurements of radial FIDA intensity profiles during on- and off-axis NBI. Section 4 gives results and a short introduction to the FIDASIM [17] code. The code enables the comparison between the measurements and the simulations, which use as inputs the fast-ion distribution functions provided by TRANSP [18]. Section 5 discusses the fast-ion redistribution due to a $q = 2$ sawtooth-like crash that ejects from the plasma center approximately 50% of the fast-ion population. Finally, conclusions are given in section 6.

## 2. FIDA diagnostic setup at ASDEX Upgrade

Figure 1 shows an overview of the FIDA diagnostic's LOS and of the NBI heating system used at ASDEX Upgrade (AUG). Two NBI injectors, with four sources each, can heat discharges with up to 20 MW of power. Box 1 (NBI 1-4) injects neutrals with a maximum energy of 60 keV and box 2 (NBI 5-8) with 93 keV. The FIDA diagnostic's 25 toroidal (roughly tangential to the magnetic field lines) LOS are focused close to the midplane on NBI 3. Fibers with a diameter of 400 $\mu$m guide the collected light outside the torus hall to a 0.28 m Czerny Turner-like spectrometer that uses lenses instead of mirrors. After passing though a tunable entrance slit, the light is dispersed by a 2400 lines mm$^{-1}$ grating and then focused on an EM-CCD camera. The camera has a 16 bit dynamic range, an array of $512 \times 512$ 16 $\mu$m pixels, and images a spectral range of about 9 nm. Typically, the camera is operated in frame transfer mode with 10 ms exposure time and the entrance slit is opened to 200 $\mu$m yielding a rectangular-shaped instrument function with a spectral width of about 0.2 nm on the CCD.
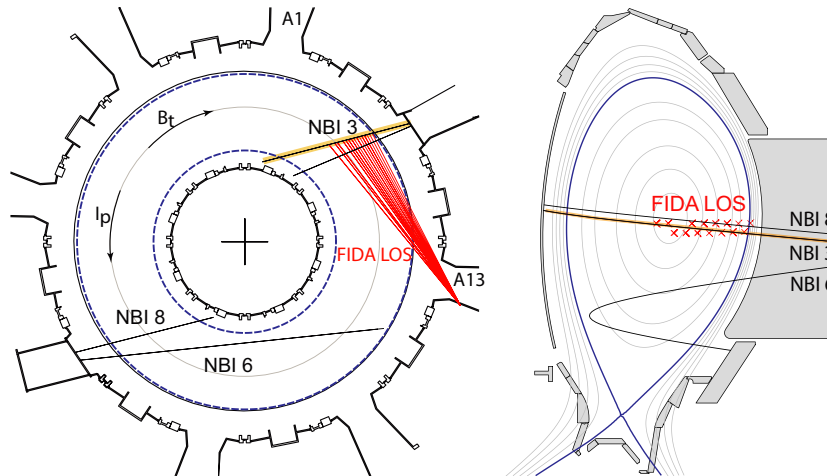
**Figure 1.** Toroidal and poloidal cross section of the AUG tokamak. The LOS of the FIDA diagnostic are focused on neutral beam source 3 (60 kV). A1 and A13 indicate the positions of two gas valves that, when turned on, influence the FIDA measurements with polluting line radiation.
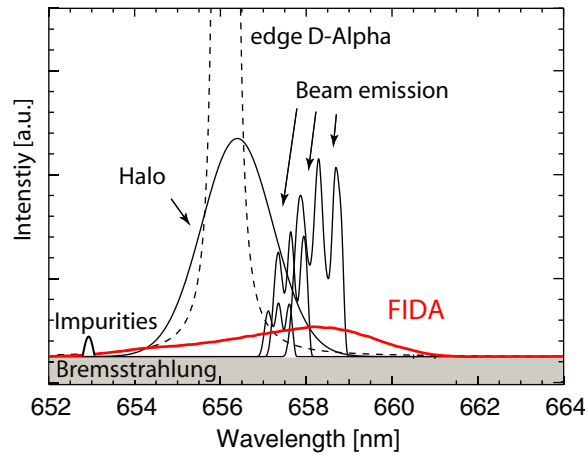


**Figure 2.** Schematic illustration of active and passive contributions present in FIDA spectra when using a toroidal diagnostic setup. The active contributions are the FIDA emission, the beam emission and the halo emission. Passive contributions are bremsstrahlung radiation, the edge D-alpha emission and line radiation from impurity ions.

The geometry of the NBI system and of the LOS, together with the nature of the FIDA radiation, provide a radial resolution of the FIDA diagnostic of about $\pm 3.5$ cm (see the appendix). Furthermore, the setup is such that most of the FIDA radiation is observed in the red-shifted wavelength range (up to 662.6 nm for $E_{\parallel} = 93$ keV). This enables FIDA measurements with good signal to noise ratios because a significant part of this spectral range (from 659.5 nm and above) does not contain superimposed bright spectral contributions.

As illustrated in figure 2, the bright active contributions (present only with NBI 3) to FIDA spectra are the halo and beam emission. The halo emission is D-alpha radiation that is emitted from NBI halo neutrals. Its spectral shape can be approximated with a Gaussian curve since the halo neutrals are thermally distributed. The spectral position of the halo emission depends
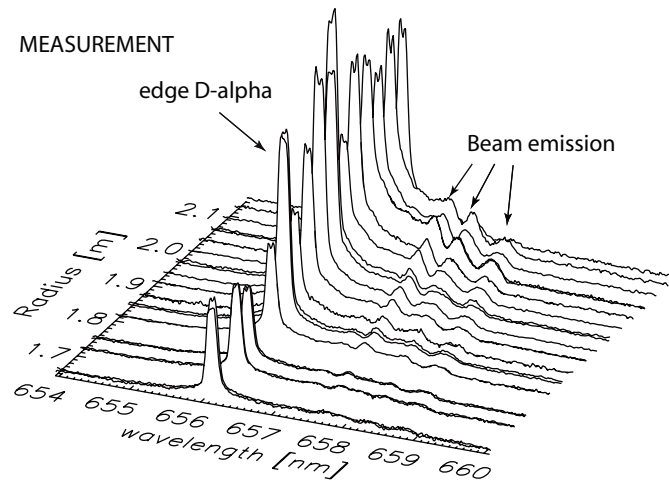
**Figure 3.** Measured D-alpha spectra as a function of intersection radius between the FIDA diagnostic's LOS and NBI 3. The spectral position of the beam emission increases toward the plasma center where the LOS are less perpendicular to NBI 3.

on the plasma rotation. In NBI heated discharges the toroidal plasma rotation is typically co-current which results in red-shifted observations of the halo emission. However, in plasmas with moderate temperatures and rotations ($T_i$ < 8 keV, $v_{tor}$ < 250 km s$^{-1}$), no significant contribution from the halo emission is expected at wavelengths above 659.5 nm.

The beam emission is D-alpha radiation, emitted by the injected beam neutrals which become excited when penetrating into the plasma. Its spectral shape depends mainly on the energy mix of the injected neutrals (full, half and third energy components), the Doppler effect and on the motional Stark effect. While the Doppler effect shifts the radiation of the full, half and third energetic neutrals in wavelength, the motional Stark effect splits each contribution into three peaks (see figure 2). The FIDA diagnostic observes the beam emission with relatively small Doppler shifts despite the high velocity of the NBI particles. The diagnostic's LOS intersect NBI 3 with angles $\alpha$ close to 90° which yield, according to equation (1), low shifts in wavelength. Figure 3 shows that the spectral position of the beam emission slightly increases for the central LOS (these are less perpendicular to NBI 3). However, the spectral region containing the beam emission never exceeds 659.5 nm.

Passive contributions to FIDA spectra (also present without NBI 3) are the bremsstrahlung and line emissions from the plasma edge. Bremsstrahlung originates from the whole plasma and appears as a flat offset in the spectra adding to the photon noise. To achieve reasonable signal to noise ratios, FIDA measurements need spectra with low levels of bremsstrahlung, i.e. discharges with low densities (below ∼7 × 10$^{19}$ m$^{-3}$ at AUG) and low $Z_{eff}$. Passive line emissions that are present in FIDA spectra are radiation from impurity ions, passive FIDA light and edge D-alpha radiation ($\lambda \sim$ 656.1 nm). The edge D-alpha emission is very bright and, therefore, cannot be measured simultaneously with the FIDA radiation; else, the diagnostic's CCD camera would saturate. Figure 4 shows measured active and passive FIDA spectra on a semi-logarithmic scale. The spectrometer grating was moved such that the edge D-alpha emission is excluded from the spectra. Only its right wing can be observed at wavelengths close to 656 nm. Line emissions from impurity ions are only present with significant intensities around 658 nm. There, two C II lines can be observed. Above 659.5 nm the passive spectrum (the background) is dominated by the flat bremsstrahlung radiation. This is in part due to the
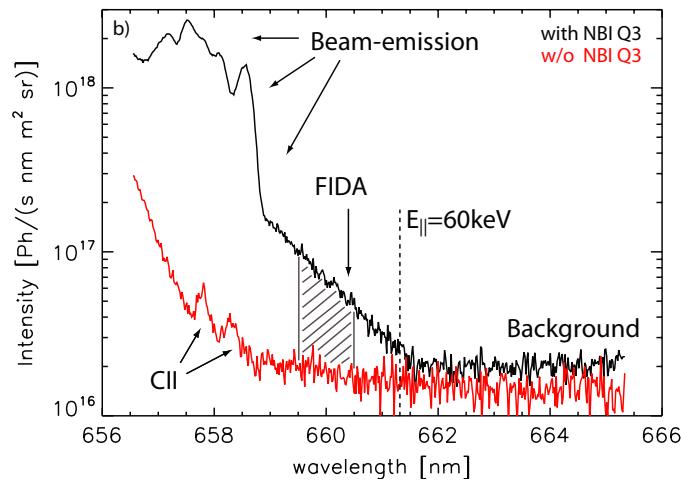
5

**Figure 4.** FIDA spectra on a semi-logarithmic scale, observed with active signal contributions from NBI 3 (black) and without (red).
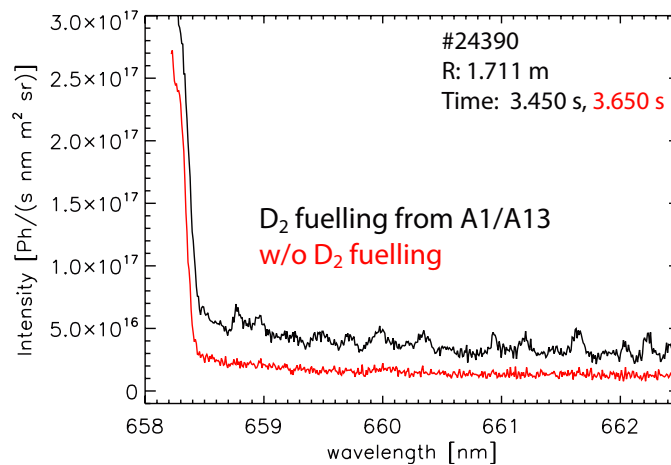


**Figure 5.** FIDA spectra observed with and without $D_2$ fueling from valves A1 and A13. Without fueling, the spectra clearly show much less polluting line radiation. The positions of the gas valves A1 and A13 are shown in figure 1.

full tungsten coated walls, which give plasmas with low levels of low-$Z$ impurities and in part due to the choice of gas fueling. It was found that changing the position of $D_2$ fueling strongly affects impurity radiation in CXRS spectra. As can be seen in figure 5, $D_2$ injection from two valves that are situated close to the FIDA diagnostic's LOS (A1 and A13, indicated in figure 1) yields an unacceptably high contamination of the spectra with additional line radiation (most likely W I lines).

Passive FIDA radiation is emitted by fast ions that undergo charge-exchange reactions with neutrals present at the plasma edge. It typically shows negligible intensities since the overlap of the fast-ion and edge neutral density profiles is small. However, significant passive FIDA radiation has been observed at AUG in discharges which feature simultaneously high edge neutral densities and large edge fast-ion populations; as, for example, in the ramp up
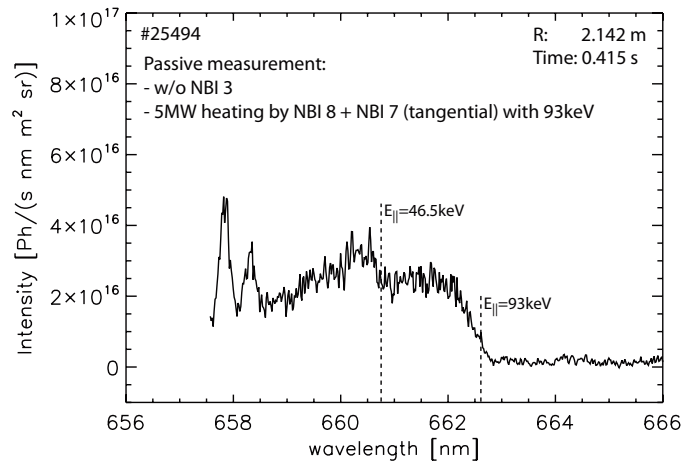
**Figure 6.** Passive FIDA spectrum observed in the ramp up phase of discharge #25494. In addition to the passive FIDA radiation, two passive C II lines are present at 657.8 and 658.3 nm.

phase of discharges with high levels of recycling that employ off-axis NBI injection. Figure 6 shows a passive spectrum measured in the initial phase of a discharge that was performed with off-axis heating. The spectrum shows distinct steps in intensity with wavelength that correspond to the full (93 keV, 662.65 nm) and half (46.5 keV, 660.66 nm) injection energies of the NBI. The measured FIDA spectrum is clearly passive in nature as NBI 3 (needed for active FIDA measurements) was off.

Profile information is obtained by integrating the spectra of the 25 LOS over a specific wavelength range (e.g. see shaded area in figure 4) and by subtracting off the contributions from passive radiation. As an example, figure 7 shows a radial FIDA intensity profile (black) that corresponds to the integration range between 659.5 and 660.5 nm ($E_\parallel$ between 25 and 42 keV). The statistical uncertainties of the profile are indicated with error bars derived from the photon noise and from the diagnostic's readout noise. Relative uncertainties in the intensity calibration of two channels that have similar viewing directions can be inferred by comparing their measured radiances. The largest difference in measured radiances of two adjacent LOS is observed at ∼1.8 m where measured photon fluxes typically differ by about 20%. In order to subtract the passive contributions from the radial FIDA intensity profiles two methods exist: first, one can make use of the beam modulation technique in which passive spectra are subtracted from the active ones. Second, one can model the passive components within the active spectra, enabling continuous measurements. At AUG, the clean FIDA spectra permit to model the passive radiation by a flat line, representing only the radiation from bremsstrahlung. Possible changes to the level of bremsstrahlung can be taken into account via this 'flat line approximation' because the level of bremsstrahlung is also observed in active spectra at wavelengths above 663 nm, where no emissions from fast ions are expected (with the exception of ICRF heated discharges). The additional systematic uncertainties, which arise in the profiles when using the flat line approximation, can be quantified in passive radial profiles, i.e. in profiles that are calculated using passive spectra from which the flat line has been subtracted. Figure 7 shows, in addition to the active radial FIDA intensity profile, a passive profile. The passive profile is not zero on average, but shows a small, positive offset, explained by weak contributions from the wing of the passive edge D-alpha emission and from passive FIDA light. The fact, that the offset is constant across all LOS, confirms its passive
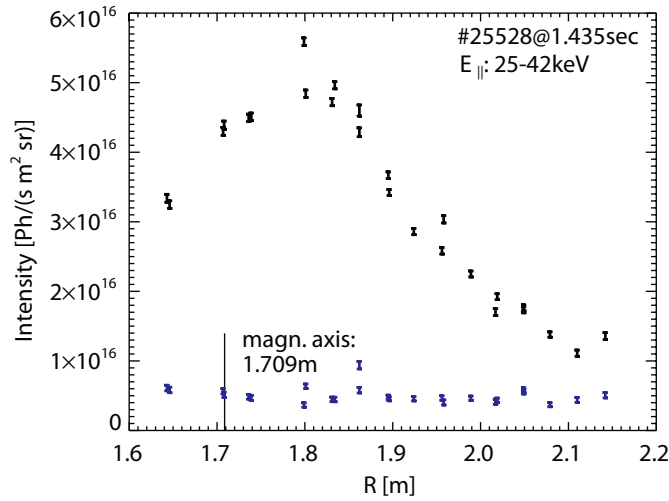
7

**Figure 7.** Radial FIDA intensity profile (black) determined by integrating the observed spectra from 659.5 to 660.5 nm (corresponding to parallel fast-ion energies, $E_\parallel$, between 25 and 42 keV). In addition, a passive intensity profile (blue) is shown that has been determined from spectra acquired without heating from NBI3. The statistical uncertainties ($\pm 1$ sigma) that originate from the diagnostic's readout noise and from the photon noise are indicated by error bars.

nature. Passive line radiation is edge localized and thus, similar for all of the FIDA LOS. Due to the offset, it is difficult to interpret the absolute quantity of the continuously observed radial FIDA intensity profiles. In particular in discharges that show edge-instabilities like ELMs, the offset changes due to changing radiances of the edge D-alpha emission. However, it is possible to study the temporal evolution of radial profiles in continuous modus even in the presence of small edge-instabilities because the shape of the radial FIDA intensity profiles is not affected.

The geometric setup of the FIDA diagnostic and the wavelength range over which the FIDA radiation is free from superimposed bright radiation determine a specific region in the velocity space in which fast ions can be monitored. To illustrate this part of the velocity space, figure 8 shows a weighting function [19] that results from a convolution of the diagnostic's geometry and instrument function with the Doppler effect, the motional Stark effect and the probability for charge exchange into the $n = 3$ level. The weighting function in figure 8 was determined for a central LOS, a wavelength range between 659.5 and 660.5 nm, a magnetic field configuration with 2.5 T (on-axis) and a typical density profile of injected and halo neutrals. As can be seen, the toroidal FIDA diagnostic observes mainly co-rotating fast ions (pitch $\sim -1$) with energies above 25 keV in a relatively small part of the velocity space. This is different from a poloidal system (LOS perpendicular to the magnetic field lines), which would observe a much larger portion of the velocity space [7]. The shifts in wavelength observed with a poloidal FIDA diagnostic would depend, in addition to the energy and pitch angle, on the 'gyro-phase' of the fast ions. Furthermore, a poloidal view would observe stronger motional Stark splitting because it would measure ions with velocity vectors perpendicular (pitch $\sim 0$) to the magnetic field lines. Hence, the observed maximum wavelength shifts would be larger and the shifts would depend on more parameters. Thereby, a larger fraction in velocity space would be monitored.

The relatively narrow and well-defined area in the velocity space that is observed by the toroidal setup used at AUG overlaps well with the fast-ion distribution functions that are present
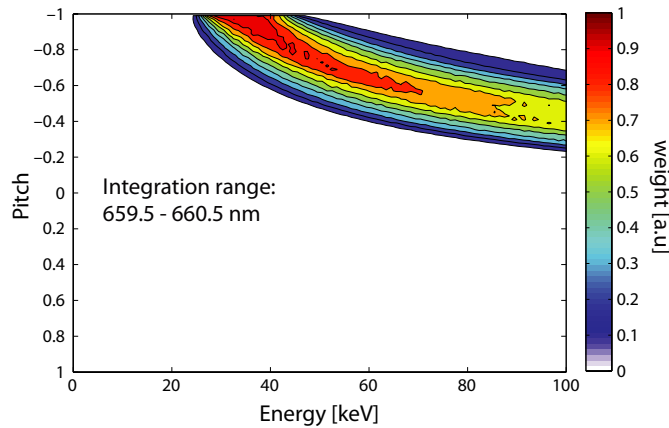
**Figure 8.** Velocity space weighting function calculated for a central line of sight of the toroidal FIDA diagnostic and for wavelengths between 659.5 and 660.5 nm.
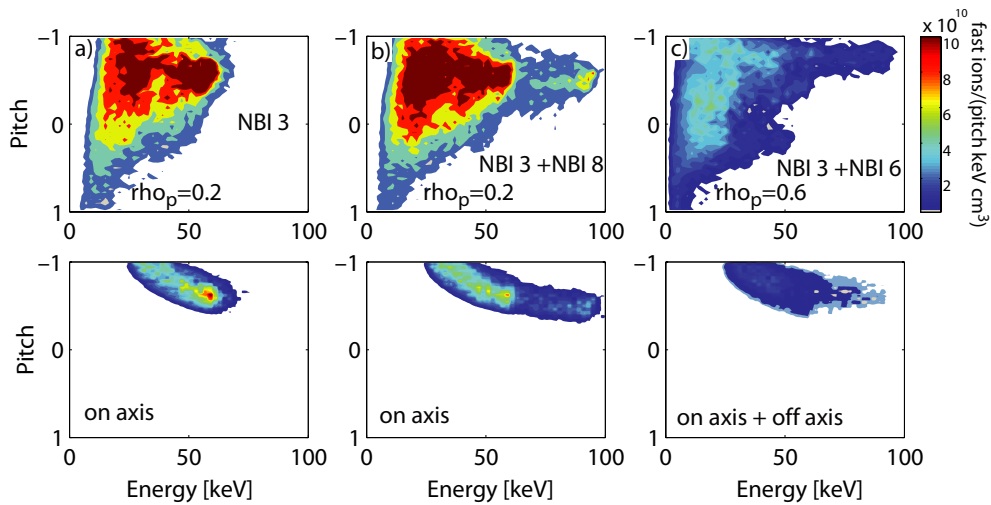


**Figure 9.** The upper figures show three different velocity space populations of fast ions injected by NBI3 (*a*), by NBI 3 and the on-axis source 8 (93 keV) (*b*), and by NBI 3 plus the off-axis source 6 (93 kev) (*c*). The lower three figures show the velocity space populations of fast ions multiplied with the diagnostic's weighting function.

in NBI heated plasmas. The top row of figure 9 shows three different TRANSP calculated fast-ion velocity distributions corresponding to three different NBI heating configurations. Figure 9(*a*) illustrates the velocity distribution of fast ions injected by NBI 3. Figures 9(*b*) and (*c*) show velocity distributions of fast ions injected by NBI 3 plus the on-axis source 8, and the off-axis source 6, respectively. The bottom row of figure 9 shows the products of the FIDA diagnostic's weighting function with the three different fast-ion velocity distributions. The products indicate the fast-ion distribution, which is really seen by the FIDA diagnostic. Consequently, the toroidal FIDA diagnostic permits the observation of fast ions injected by the AUG NBI system as its weighting function clearly overlaps with a significant fraction of the fast-ion distribution function.
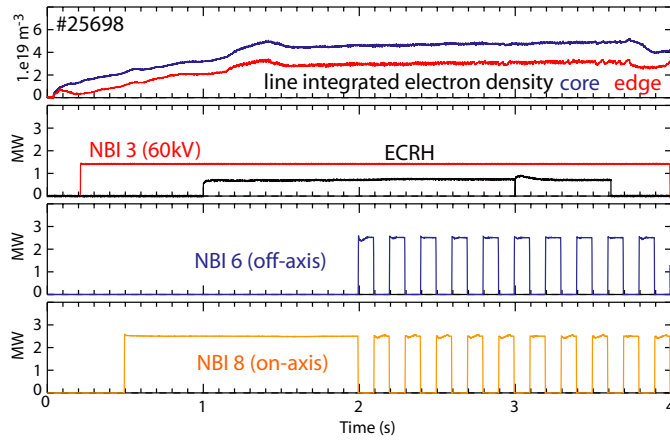
**Figure 10.** Time traces of discharge #25698 ($B_t = 2.5$ T, $I_p = 0.8$ MA) in which on- and off-axis heating NBI sources are modulated with a period of 200 ms.
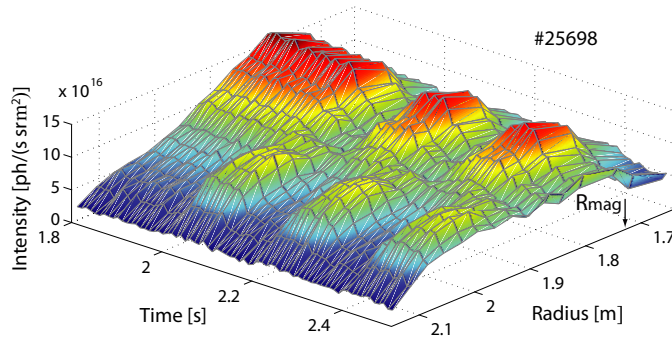


**Figure 11.** Radial FIDA intensity profiles for $E_{\parallel}$ between 25 and 42 keV as a function of time. Starting at 2.0 s, on- and off-axis NBI heating is modulated.

## 3. Analysis of on-axis and off-axis NBI deposition with FIDA

The effect of different NBI heating schemes on the fast-ion distribution function has been studied by analyzing radial FIDA intensity profiles. Discharge #25698 was performed with modulation of NBI sources 8 (on-axis) and 6 (off-axis) in addition to continuous operation of source 3 (needed for active FIDA measurements). As can be seen in figure 10, the discharge had a core line integrated density of about $4.5 \times 10^{19}$ m$^{-3}$, 4 MW of NBI heating and 0.5 MW of ECRH heating. Starting at 2.0 s the on- and off-axis NBI sources were alternated with a period of 200 ms such that the total power was kept constant. Radial FIDA profiles were analyzed for every acquired time frame and are shown in figure 11. To produce these profiles, the spectra were integrated over the wavelength range from 659.5 to 660.6 nm. The changes in the radial fast-ion distribution caused by the different injection geometries of sources 8 and 6 can be observed well due to the 10 ms temporal resolution of the FIDA diagnostic and the ability to make continuous measurements. The profiles clearly show peaked radiance in the plasma core when NBI 8 is on. When source 6 is exchanged for source 8 the core FIDA radiance decreases and increased radiation is observed toward the plasma edge. This demonstrates the off-axis character of source 6 while source 8 is mainly on-axis.
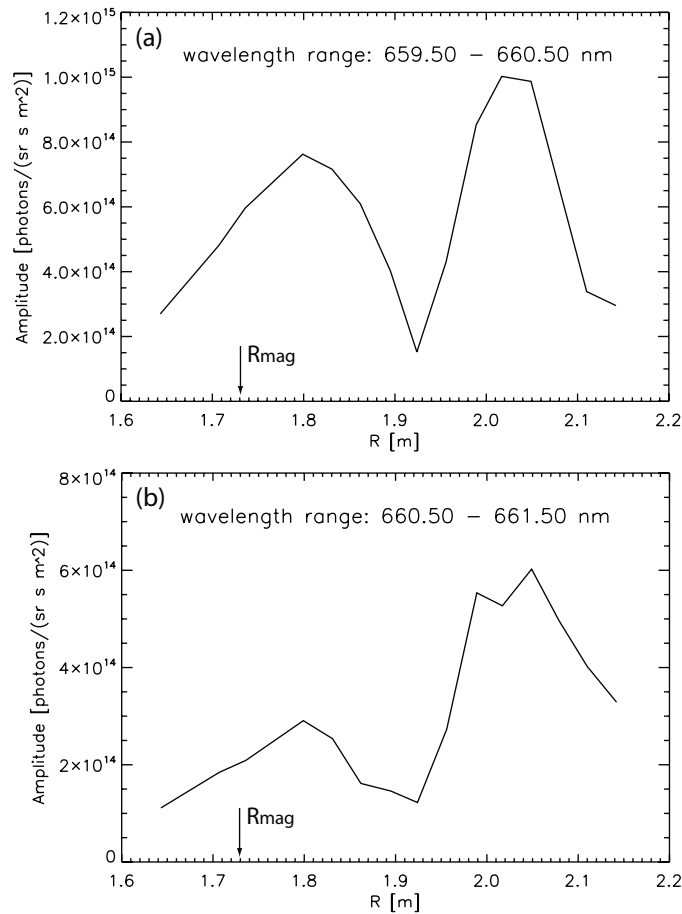
**Figure 12.** Radial FIDA amplitude profiles from discharge #25698 between 2.0 and 3.5 s. By changing the wavelength interval used to determine the radial profiles, different parts of the fast-ion velocity space population are viewed.

Furthermore, the influence of the injection angles of sources 8 (perpendicular) and 6 (tangential) (see figure 1) on the FIDA measurement can be demonstrated by changing the wavelength integration range used to calculate the radial FIDA profiles. The wavelength range determines which part of the velocity space is observed and hence, changes the diagnostic's weighting function. A Fourier analysis using the frequency of the modulation of sources 6 and 8 has been applied between 2.0 and 3.5 s to improve the signal to noise ratio in the radial FIDA profiles because the FIDA radiance becomes weak at increased wavelength ranges. Resulting radial FIDA amplitude profiles are shown in figures 12(*a*) and (*b*); these correspond to the wavelength ranges 659.5–660.5 nm and 660.5–661.5 nm, respectively. Two radially separated peaks exist which can be related to on- and off-axis heating. By comparing figures (*a*) and (*b*), the tangential character of the off-axis source becomes evident. The ratio between the off-axis and on-axis peak is larger for the higher wavelength range, due to the different injection angles. The more tangentially injected fast ions from the off-axis source (compare figures 9(*a*) and (*c*)) have smaller angles, $\alpha$, to the diagnostic's toroidal LOS and therefore emit D-alpha radiation at higher wavelengths. Hence, they contribute more when integrating over higher wavelength ranges.
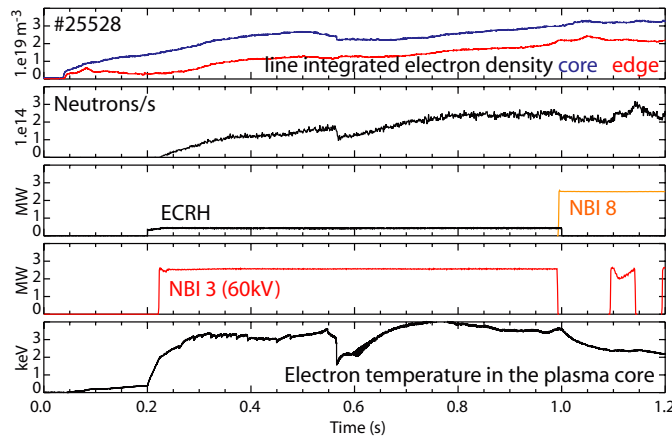
**Figure 13.** Time traces of discharge #25528. NBI 3 injects continuously between 0.2 and 1.0 s. At 0.565 s, a sawtooth-like crash leads to a drop in the core electron temperature and in the neutron rate which is discussed in section 5.

## 4. FIDA measurement compared with simulation code results

The interpretation of FIDA measurements is rather challenging. It is complicated by the nature of the FIDA radiance, which makes the direct conversion to a fast-ion distribution function very difficult. However, for a specific fast-ion distribution function, the FIDA spectrum can be predicted and then compared with the measurement. For this purpose, a Monte Carlo simulation code, FIDASIM [17], has been implemented. FIDASIM works on a three-dimensional simulation grid and solves the collisional–radiative model time dependently. The code contains atomic rates and cross sections, the NBI parameters (geometry, power, energy, species mix) and the FIDA diagnostic's geometry. As inputs, it needs to be provided with information on the fast-ion distribution function, the magnetic equilibrium, and on kinetic plasma profiles. Three-dimensional density profiles of injected neutrals and beam emission spectra are determined by simulating the attenuation, excitation and photon emission of injected neutrals. Halo neutrals, which are born by charge exchange between the injected neutrals and the bulk plasma, are also simulated. The neutral density profiles are then used to determine the probability for charge exchange with Monte Carlo markers that represent a fast-ion distribution function. The FIDA emission is then calculated by following the path of neutralized fast ions and by accounting for the Doppler and motional Stark effects. The code finally yields synthetic spectra containing the halo emission, the beam emission, and the FIDA emission, whereas passive contributions are not taken into account.

To compare measurement and simulation, a 0.8 MA discharge with low heating power was chosen (2.5 MW of NBI heating and 0.5 MW of ECRH) in which the fast-ion diffusivity is expected to be classical (no anomalous transport) [20]. As shown in figure 13, the discharge had a low electron density ($(3–4) \times 10^{19}$ m$^{-3}$) and NBI 3 operates continuously from 0.2 s on. At 0.985 s, only the on-axis source NBI 3 injects fast ions in an MHD-quiescent plasma. The FIDASIM code was applied at this time point using a classical fast-ion distribution provided by TRANSP. In figures 14(*a*) and (*b*) two resulting simulated spectra, corresponding to two different radial positions, are compared with the measurement. The simulated beam, halo, and FIDA emission have all been scaled by a constant factor of 1.3 for every channel. This factor, which is needed to match simulation and measurement, can be explained best by uncertainties in the data such as the intensity calibration of the diagnostic or by uncertainties in the simulation
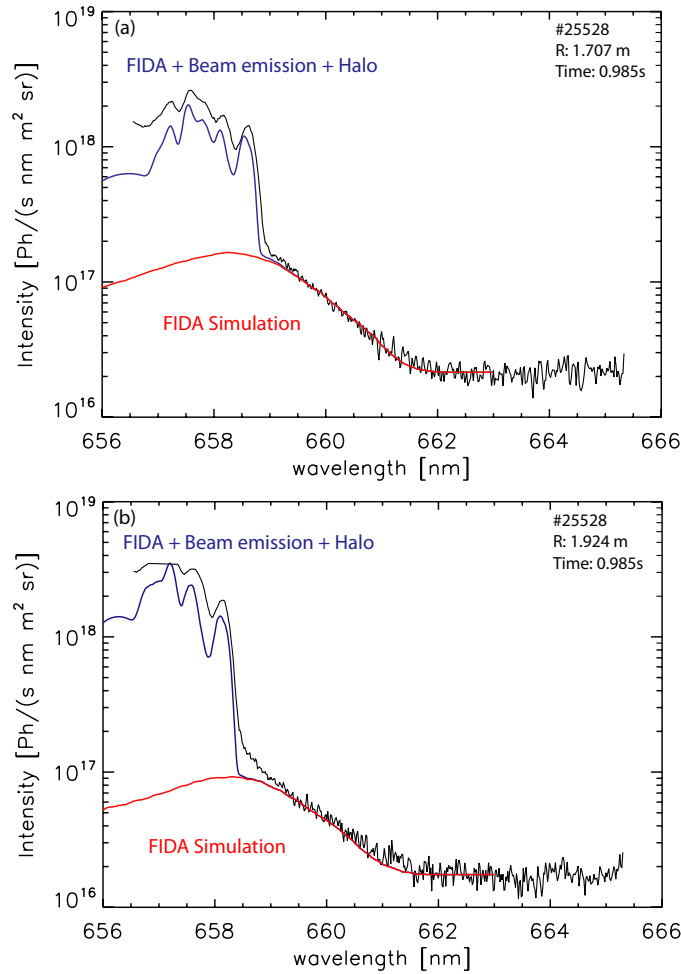
**Figure 14.** Comparison of measured FIDA spectra (black) to FIDASIM results during on-axis NBI heating at two different radial positions (1.707 m (*a*) and 1.924 m (*b*)). In red, the simulated FIDA components are shown. The sum of simulated beam emission, FIDA and halo components is shown in blue. The simulation results have been scaled up by 30%.

code (e.g. the atomic rates and cross sections). The spectral shape of the simulated emission fits very well to the measurement (not only the FIDA emission itself, but also the sum of the FIDA, beam and halo emission). This good agreement indicates that the fast-ion velocity distribution provided by TRANSP is consistent with the data.

For the classical fast-ion distribution function, good agreement has also been found between simulated and measured radial profiles. Figure 15(*a*) shows three different simulated fast-ion density profiles (summed over all pitches and energies) from TRANSP that correspond to different levels of global fast-ion diffusion. The red profile corresponds to the classical distribution without additional diffusion, the blue one to $0.5 \, \mathrm{m^2 \, s^{-1}}$ additional fast-ion diffusion and the green profile to an additional fast-ion diffusion of $1.0 \, \mathrm{m^2 \, s^{-1}}$. Corresponding artificial FIDA intensity profiles are compared with the measurement in figure 15(*b*). The profiles, which were determined by integrating the spectra from 659.5 to 660.5 nm ($E_{||}$ between 25 and 42 keV), have been scaled by the factor of 1.3 mentioned above. The shape of the synthetic
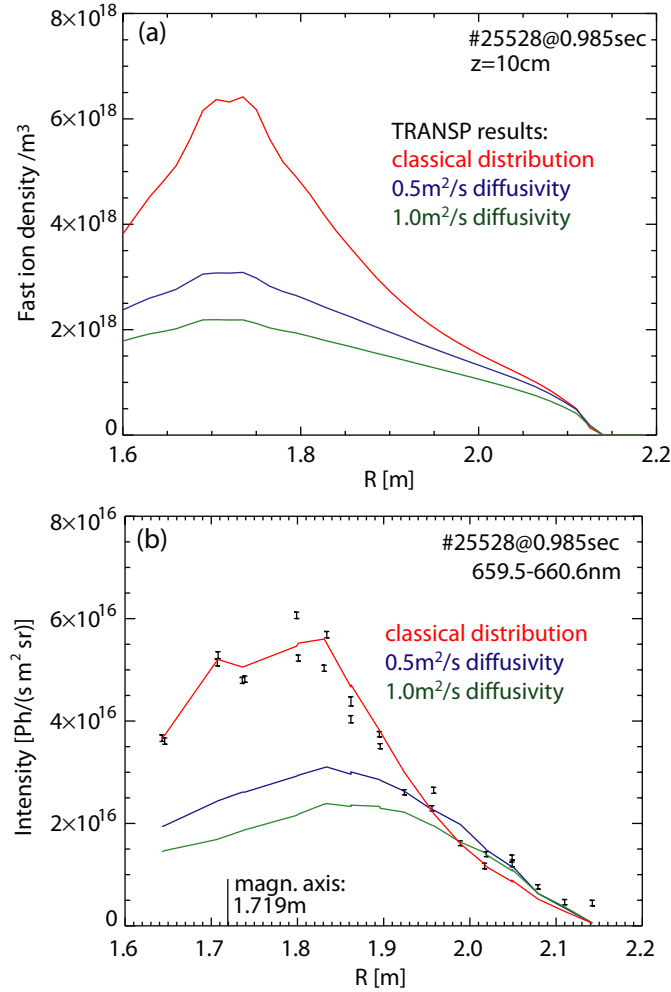
**Figure 15.** (*a*) Radial fast-ion density profiles (in the $z = 10$ cm plane and summed over pitch and energy) provided by TRANSP that correspond to different global fast-ion diffusion coefficients. (*b*) Comparison of a measured FIDA intensity profile (black, error bars) with artificial profiles, corresponding to different levels additional fast-ion diffusion as calculated by FIDASIM (lines). The profiles correspond to $E_{\parallel}$ between 25 and 42 keV. The passive radiation has been subtracted from the measured profile using a background frame, acquired at 1.015 s. The error bars show the statistical uncertainties of the measurement which originate from the diagnostic's readout noise and from the photon noise.

profile which represents the classical fast-ion distribution function fits reasonably good to the measurement whereas the anomalous diffusion tends to flatten the simulated profiles as expected. This permits us to conclude that the classical fast-ion distribution function predicted by TRANSP is consistent with the data in the case of MHD-quiescent plasmas with low heating power.

## 5. Measurement of a MHD induced fast-ion redistribution

The clean FIDA spectra at AUG enable the study of the temporal evolution of the fast-ion profiles in the presence of MHD instabilities. A fast-ion redistribution during a sawtooth-like
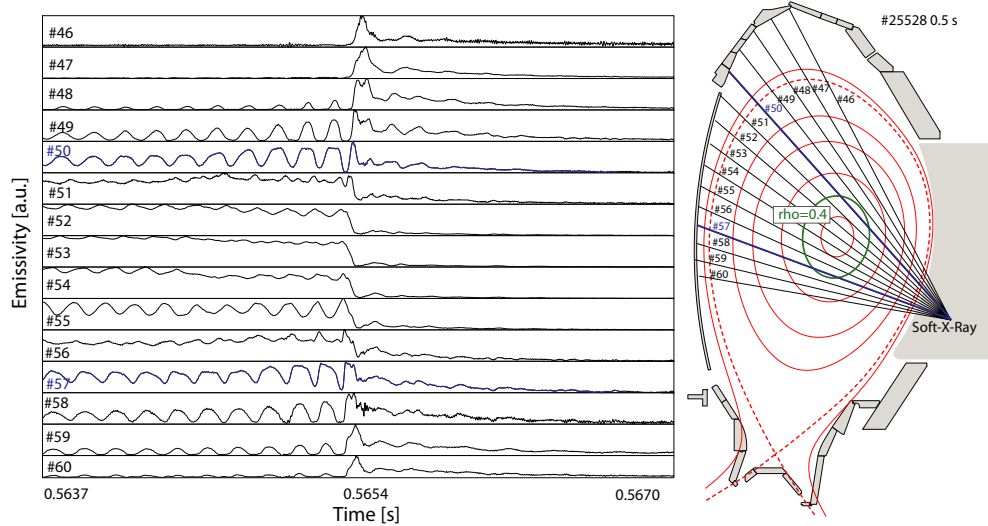
**Figure 16.** Soft-x-ray measurement during a sawtooth-like crash. The geometry of the soft-x-ray channels is shown on the right. The inversion radius on the crash can be related to about $rho_{tor} = 0.4$.

crash has been observed and is presented in this section. Sawtooth crashes are well known to strongly affect the confinement of passing ions [21, 22] and, therefore, are ideal candidates to explore the FIDA diagnostic's capabilities. The crash is observed in discharge #25528 around 0.565 s. It is caused by the overlapping of two (2,1) tearing modes which were able to exist because the discharge had a reversed $q$-profile. The overlap of these two modes probably leads to stochastization of the magnetic field lines which is consistent with the observed fast temperature redistribution. The drop of the core electron temperature can be seen in figure 13. Soft-x-ray [23] measurements of the crash localize its inversion radius to about $rho_{tor} = 0.4$ (normalized radius) and are shown in figure 16.

Similar events have been observed previously at TFTR and were identified as $q = 2$ off-axis sawtooth crashes [24]. The influence of the crash on the FIDA measurement can be seen easily in the measured spectra and profiles. Figure 17 shows spectra from a central line of sight (*a*) and radial FIDA profiles (*b*) before (black) and after (red) the sawtooth-like crash. The core FIDA radiance is clearly lower after the MHD event while the radiance at the plasma edge increases. This indicates a redistribution of fast ions.

However, a direct interpretation of the FIDA spectra and radial intensity profiles can be difficult. The sawtooth-like crash changes the kinetic plasma profiles which influence the density of injected and halo neutrals along the path of source 3. Consequently, the probability of fast ions to undergo charge-exchange reactions, i.e. the FIDA radiance, might be affected. To account for changes of the kinetic plasma profiles, we calculated approximate fast-ion density profiles from the FIDA measurement. Using the FIDASIM code, density profiles of injected and halo neutrals can be determined for every acquired time frame. This enables us to calculate a time-dependent probability for fast ions to undergo charge-exchange reactions. Using the Einstein coefficients and by accounting for the geometry of the FIDA diagnostic's LOS approximate fast-ion densities can then be determined. Three assumptions are needed when calculating approximate fast-ion densities: first, the fast-ion density is assumed to be constant along the intersection of the LOS with the NBI. Second, it is necessary to assume that the FIDA radiation is emitted directly after charge exchange (only a small fraction of
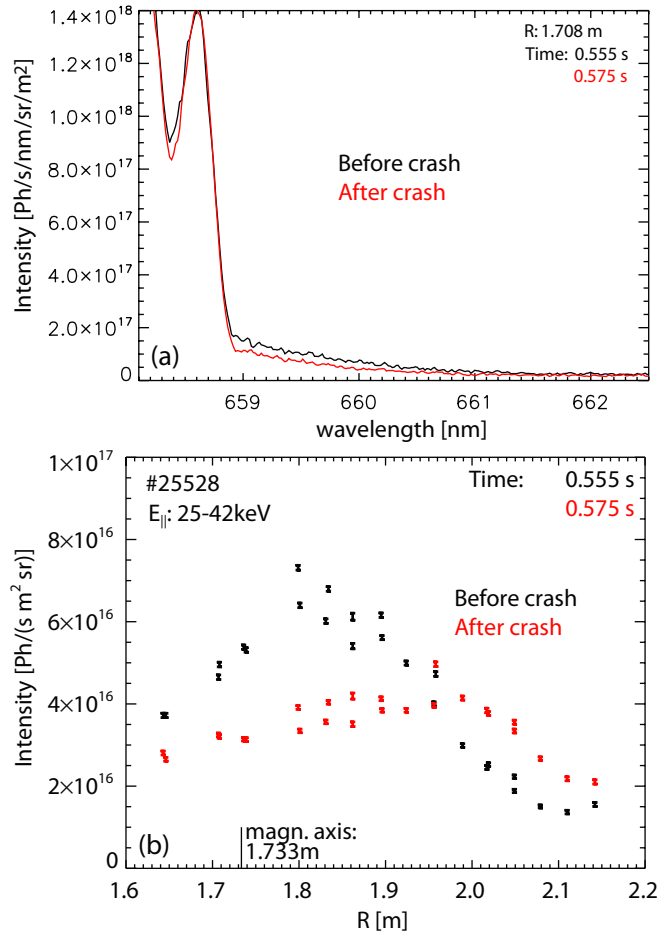
15

**Figure 17.** FIDA spectra (*a*) and radial intensity profiles (*b*) observed before and after a sawtooth-like crash. The profiles, calculated using the flat line approximation to account for the passive radiation, indicate that the core FIDA radiance is lowered after the crash while the radiance at the plasma edge increases. The error bars indicate the statistical noise of the measurement.

the FIDA radiation is emitted later along the path of a fast neutral as discussed in section 1). Third, a constant fast-ion velocity vector must be assumed when calculating the probability for charge exchange because FIDA measurements, as discussed in section 1, do not resolve independent information on the energy and direction of fast ions. When selecting a constant fast-ion velocity vector, the toroidally viewing FIDA diagnostic is advantageous. Its narrow weighting function (see figure 8) permits us to define a fast-ion velocity vector that represents the observed fast-ion velocity space population well (pitch of $-0.8$, $35$ keV). It should be noted that these three approximations make an interpretation of the absolute quantities of the approximate fast-ion densities difficult. However, the dynamics of the fast-ion distribution viewed by the toroidal FIDA diagnostic can be studied.

The temporal evolution of the approximate fast-ion density profiles in the presence of the sawtooth-like crash can be seen in fast figure 18. The profiles have been mapped on magnetic flux coordinates, $\rho_{tor}$, in order to account for possible variations of the plasmas' shape and position. From figure 18 it is clear that the sawtooth-like crash ejects approximately 50% of
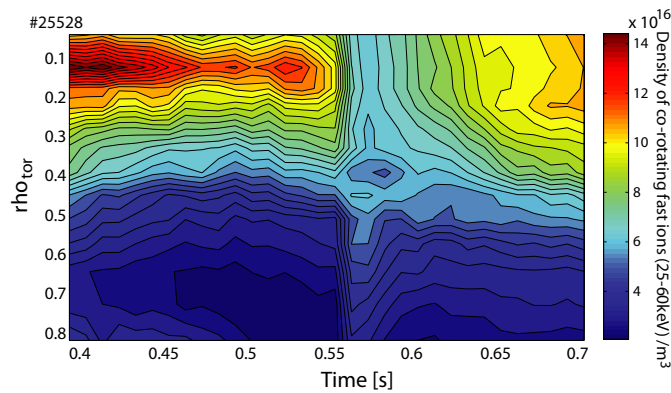
**Figure 18.** Temporal evolution of approximated fast-ion density profiles of mainly co-rotating fast ions with energies between 25 and 60 keV from discharge #25528. At 565 ms a sawtooth-like crash caused by a (2,1) double tearing mode redistributes fast ions toward the plasma edge.

the fast-ion population from the plasma center and redistributes the fast ions toward the plasma edge. The inversion radius of the crash can be located with the FIDA measurement at about $\text{rho}_{tor} = 0.4$. This is in good agreement with the soft-x-ray measurement. Moreover, FILD measurements agree with the FIDA measurement in so far as strong losses of fast ions are observed during the crash. A detailed analysis of the physics mechanism responsible for this strong redistribution and the observed fast-ion losses is the subject of an upcoming publication.

## 6. Conclusion

The FIDA technique with toroidally viewing LOS has been successfully applied to NBI heated plasmas in the full tungsten AUG tokamak. The combination of the NBI and diagnostic's geometry allow the measurement of relatively small changes of the fast-ion phase-space population due to a narrow weighting function in the velocity space. In general, in AUG the background emission can be subtracted as a flat offset without beam modulation due to the low contamination of the FIDA spectra with impurity lines. Thus, the temporal evolution of the fast-ion spatial distribution can be studied in the presence of MHD instabilities.

Radial FIDA profiles for on- and off-axis NBI heating have been measured with high spatial resolution. By changing the integration wavelength range used to calculate the radial FIDA intensity profiles one can study different parts of the fast-ion velocity space. When comparing the shape of the measured radial FIDA intensity profiles with the shape of simulated profiles, good agreement in MHD-quiescent plasmas with low heating power was found for the classical fast-ion distribution function. Finally, the good time resolution of the diagnostic allowed the experimental observation of a strong redistribution of fast ions due to a $q = 2$ sawtooth-like crash.

## Appendix

The radial resolution of a FIDA diagnostic depends on the nature of the FIDA emission, on the geometry of the diagnostic's LOS and on the geometry of the NBI, i.e. the spatial extent of the 3D density of halo and beam neutrals. It can be determined using the FIDASIM code, described in more detail in section 5. FIDASIM is a Monte Carlo code that simulates the
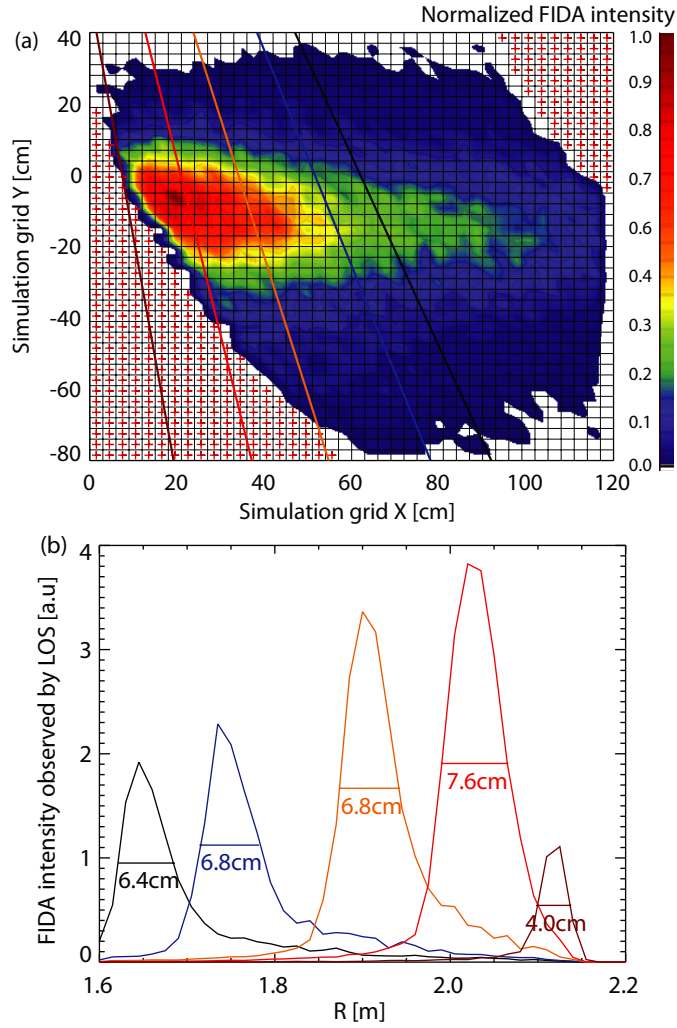
**Figure 19.** (*a*) Top-down view of the normalized, simulated FIDA photon flux in the $z = 0$ plane on the FIDASIM simulation gird. The simulation grid is oriented along the axis of NBI box 1. The red crosses mark radial positions that are located outside the last closed flux surface. Moreover, five representative lines of sight of the FIDA diagnostic at AUG are given. (*b*) The simulated photon fluxes, observed by the five LOS as a function of neutralization radius of the fast ions. The full width half maximum of the radial photon flux profiles indicate the radial resolution of the FIDA diagnostic, which is on average about $\pm 3.5$ cm.

spectral emission of fast ions on a three-dimensional grid. For every simulated fast ion, the radial position where it is neutralized and the position where it contributes to a given LOS can be determined. Hence, the radial resolution of a diagnostic can be obtained by analyzing the simulated spectral radiances per LOS as a function of the neutralization radius of fast ions.

The kinetic profiles of discharge #25528 at 0.985 s have been taken as inputs to FIDASIM to determine the radial resolution of the FIDA diagnostic at AUG. Furthermore, a constant fast-ion distribution function has been used (constant in position, pitch and energy between 10 keV and 100 keV). Figure 19(*a*) shows a top-down view of the simulated, normalized FIDA photon fluxes on the FIDASIM simulation grid. Furthermore, the viewing directions of five

representative LOS of the FIDA diagnostic are given. Figure 19(*b*) shows the simulated, normalized photons fluxes per LOS as a function of neutralization radius. As can be seen from the full width at half maximum of the radial profiles, the radial resolution of the FIDA diagnostic is on average about $\pm 3.5$ cm.

## References

[1] Fasoli A *et al* 2007 *Nucl. Fusion* **47** 264–84
[2] Garcia-Munoz M, Fahrbach H U, Zohm H and the ASDEX Upgrade team 2009 *Rev. Sci. Instrum.* **80** 053503
[3] Hutchinson I H 1987 *Principles of Plasma Diagnostics* (New York: Cambridge University Press)
[4] Kiptily V G *et al* 2002 *Nucl. Fusion* **42** 999–1007
[5] Bindslev H, Hoekzema J A, Egedal J, Fessey J A, Hughes T P and Machuzak J S 1999 *Phys. Rev. Lett.* **83** 3206–9
[6] Hellesen C *et al* 2010 *Plasma Phys. Control. Fusion* **52** 085013
[7] Heidbrink W W, Burrel K H, Luo Y, Pablant N A and Ruskov E 2004 *Plasma Phys. Control. Fusion* **46** 1855–75
[8] von Hellermann M G, Core W G F, Frieling J, Horton L D, König R W T, Mandl W and Summers H P 1993 *Plasma Phys. Control. Fusion* **35** 799–824
[9] Luo Y, Heidbrink W W, Burrell K H, Kaplan D H and Gohil P 2007 *Rev. Sci. Instrum.* **78** 033505
[10] Delabie E, Jaspers R J E, von Hellermann M G, Nielsen S K and Marchuk O 2008 *Rev. Sci. Instrum.* **79** 10E522
[11] Osakabe M *et al* 2008 *Rev. Sci. Instrum.* **79** 10E519
[12] Heidbrink W W, Bell R E, Luo Y and Solomon W 2006 *Rev. Sci. Instrum.* **77** 10F120
[13] Heidbrink W W, Park J M, Murakami M, Petty CC, Holcomb C and Van Zeeland M A 2009 *Phys. Rev. Lett.* **103** 175001
[14] Heidbrink W W *et al* 2007 *Phys. Rev. Lett.* **99** 245002
[15] Heidbrink W W, Murakami M, Park J M, Petty C C, Van Zeeland M A, Yu J H and McKee G R 2009 *Plasma Phys. Control. Fusion* **51** 125001
[16] Isler R C 1994 *Plasma Phys. Control. Fusion* **36** 171–208
[17] Heidbrink W W, Liu D and Ruskov E 2011 *Commun. Comput. Phys.* **10** at press
[18] Pankin A, McCune D, Andre R, Bateman G and Kritz A 2004 *Comput. Phys. Commun.* **159** 157–84
[19] Heidbrink W W, Luo Y, Muscatello C M, Zhu Y and Burell K 2008 *Rev. Sci. Instrum.* **79** 10E520
[20] Günter S *et al* 2007 *Nucl. Fusion* **47** 920–8
[21] Van Zeeland M *et al* 2010 *Nucl. Fusion* **50** 084002
[22] Kolesnichenko Y I and Yakovenko Y V 1996 *Nucl. Fusion* **36** 159–73
[23] Igochine V, Gude A and Maraschek M 2010 *IPP Report* 1/338, see http://edoc.mpg.de/display.epl?mode=doc&id=476537
[24] Chang Z *et al* 1996 *Phys. Rev. Lett.* **77** 3553–6